

Time-Resolved Single Dopant Charge Dynamics in Silicon

M. Rashidi^{1,2*}, J. A. J. Burgess^{3,4}, M. Taucer^{1,2}, R. Achal¹, J. L. Pitters²,
S. Loth^{3,4}, and R. A. Wolkow^{1,2}

¹Department of Physics, University of Alberta, Edmonton, Alberta, T6G 2J1, Canada.

²National Institute for Nanotechnology, National Research Council of Canada, Edmonton, Alberta, T6G 2M9, Canada.

³Max Planck Institute for the Structure and Dynamics of Matter, 22761 Hamburg, Germany.

⁴Max Planck Institute for Solid State Research, 70569 Stuttgart, Germany.

*Correspondence to:rashidi@ualberta.ca

As the ultimate miniaturization of semiconductor devices approaches, it is imperative that the effects of single dopants be clarified. Beyond providing insight into functions and limitations of conventional devices, such information enables identification of new device concepts. Atomically resolved, electronic pump-probe scanning tunneling microscopy permits unprecedented, quantitative measurement of time-resolved single dopant ionization dynamics. We use time-resolved scanning-tunneling-microscopy and spectroscopy to probe and study transport through a dangling bond on silicon before the system relaxes or adjusts to accommodate an applied field. Tunneling through the surface dangling bond makes feasible what would otherwise be too weak a signal to observe. Distinct ionization and neutralization rates of a single dopant are measured and the physical process controlling those are identified.

Understanding the fundamental properties of individual dopants locally coupled to electronic transport in semiconductors is the focus of much current research (1). This area of inquiry holds promise for new semiconductor device applications at the ultimate level of miniaturization, as well as for utilization of the quantum properties of individual impurities (2). Scanning tunneling microscopy (STM) has enabled significant progress in this field, including observation of the influence of single dopants on the local density of states (LDOS) (3–6) and local magnetic properties (7, 8) of the host semiconductor. Measurements on GaAs have shown slow dopant dynamics can be observed locally with millisecond timescale STM (9). Dynamics must exist on much faster time scales as well, but have not yet been observed using STM. Time-resolved STM (TR-STM), pioneered by Nunes and Freeman (10), has recently seen a resurgence of interest (11–15) following the application of a simplified all-electronic technique to the measurement of spin dynamics in adatoms (16). Thus far, this method has only been applied to other magnetic adatom systems (12) and atomically assembled nanomagnets (13).

Here, we measure single electron charge dynamics of individual subsurface dopants with time-resolution well beyond the limitations of conventional STM. We perform point measurements, drawing current through a surface dangling bond (DB) on a hydrogen terminated arsenic-doped Si(100)-2×1 sample with a dopant depletion layer at its surface. Dopants and the DB are decoupled from the bulk by this layer. Unlike the hydrogen terminated regions of the surface, which are passivated, the spatially extended DB orbital provides strong overlap to both the tip orbital and via vibronic coupling to the bulk bands (17), greatly enhancing sensitivity to

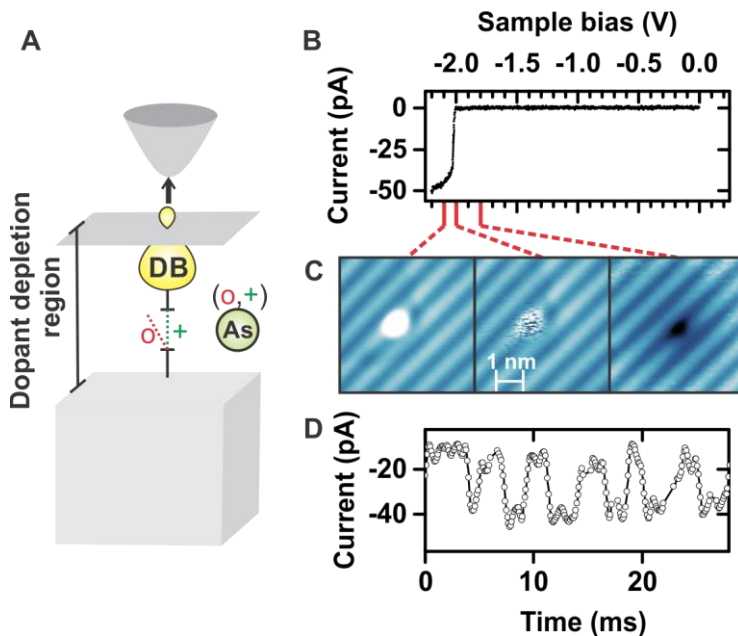


Fig. 1. Characteristic spectroscopic behavior of dangling bonds on Si samples heated to 1250°C. (A) Simple diagram of the system of study representing the dopant as an on and off switch for electron conduction from the bulk conduction band to the dangling bond through the dopant depletion region as it changes from ionized to neutral. (B) Constant-height filled-state conductance spectrum measured over a dangling bonds. (C) Constant-current STM images of the dangling bonds beyond (-2.1 V), at (-1.8 V) and before the critical voltage range (-2.0 V) at left, right, and center respectively. (D) Current time-trace at the critical voltage (-2.01V) exhibiting telegraph noise behavior at millisecond timescales.

single dopant effects. Ionization of a dopant in the electric field of the tip opens a conductance channel from the conduction band (CB) to the tip via the surface DB. This allows detection of the dopant charge state in a method analogous to a single atom gated transistor: the bulk acts as the source, the DB (strongly coupled to the tip) is the drain, and the dopant is the gate (Fig. 1 A). A combination of fast real-time acquisition and pump-probe techniques enables temporal mapping of the local dopant dynamics from nanoseconds to seconds by exploiting the DB amplification of the single dopant effects.

The Si(100)- 2×1 surface is composed of rows of silicon dimers which appear as bars in Fig. 1C. The surface is unpinned and the dimers are preserved upon termination by hydrogen. As a result of flashing to 1250°C our sample is depleted in the near surface region of dopants (a depth of ~ 60 nm measured by secondary ion mass spectroscopy (SIMS)) (18). Scanning tunneling spectra (I(V) measurements) of DBs on samples with the dopant depletion region are correlated with a sharp current onset (Fig. 1B) at a critical filled-state bias voltage (19). As the sample bias is swept more negative the appearance of the DB changes from dark with a spatially extended halo to bright, indicating drastic increase in the supply of current from bulk to DB. In the critical voltage range (middle panel in Fig. 1C), some DBs appear striped and exhibit stochastic two-state switching between low conductance (LC) and high conductance (HC) states at millisecond timescales (Fig. 1D and 2A). The observed switching rates are much slower than

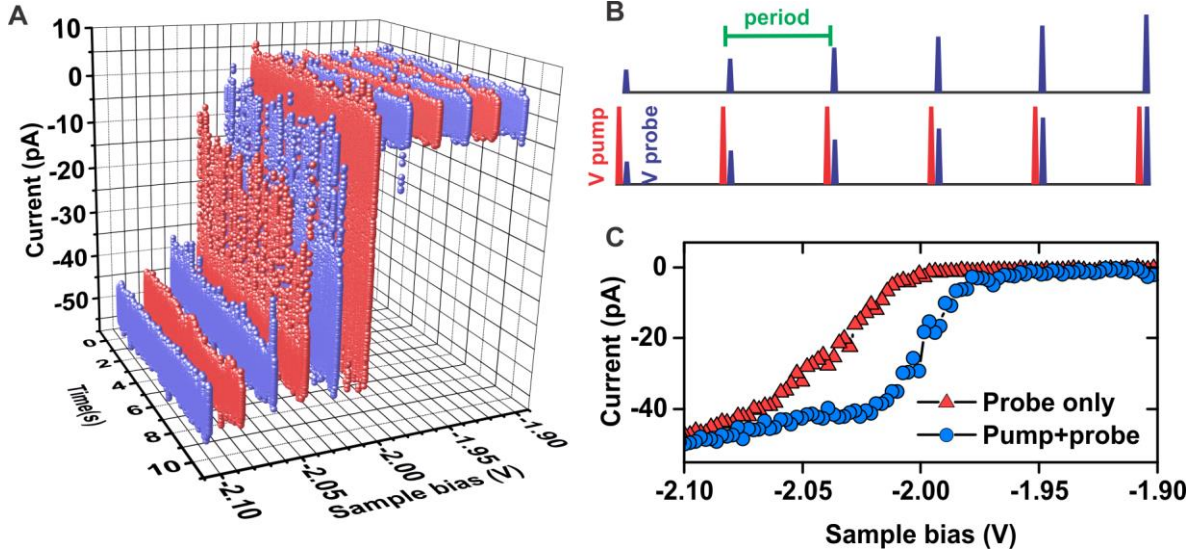


Fig. 2. Time-resolved scanning tunneling I(V) spectroscopy (TR-STs). (A) Current-time traces in the critical bias range in Fig. 1B, acquired with the maximum sampling rate of the STM controller (~ 10 kHz). Alternating colors are used for better visualization. (B) Schematic of TR-STs pulse timing: Tunneling current is measured from a series of varying-amplitude probe-pulses (blue) with and without a preceding pump pulse (red) (C) TR-STs with $1 \mu\text{s}$ probe pulses with (blue circles) and without (red triangles) a preceding $1 \mu\text{s}$ pump pulse. The DC bias voltage is set at -1.80 V. The amplitude of the pump pulse is 0.40 V and that of the probe pulse is swept from 100 to 300 mV. The relative delay between the trailing edge of the pump and the leading edge of the probe pulse is 10 ns. The observed hysteresis in TR-STs overlaps the bias range over which the system is bistable.

the rate of electrons transfer through the DB (tunneling current of ~ 40 pA). Therefore, unlike switching previously observed at positive sample bias voltages (20), these transitions cannot be caused by charge fluctuation of the DB itself. The switching could, however, be explained by charge fluctuations of a nearby dopant gating a conduction channel from the bulk to the DB (Fig. 1A). These rates are at the limit of the STM's current preamplifier, making it impossible to detect fluctuations beyond this timescale.

All-electronic pump-probe STM resolves this issue. Figure 2B displays a schematic of time-resolved I(V) spectroscopy using pump-probe methods. Instead of sweeping the DC bias voltage as in standard I(V) spectroscopy, we keep the DC bias fixed and sweep the amplitude of a train of fast microsecond scale voltage pulses. Preceding each probe pulse, a large fixed amplitude pump pulse transiently disturbs the system. The delay between pump and probe is fixed such that the pulses do not overlap. Thus the transient state immediately resulting from the pump is interrogated by the probe. Comparison to an equivalent curve measured with no pump pulse reveals any triggered dynamics. The DB shown in Fig. 1, exhibits deviations between the two curves starting at the critical voltage, -2.0 V, and extending up to -2.10 V. By contrast, the slow telegraph noise is only observed up to -2.05 V, indicating the presence of additional nanosecond scale dynamics (Fig. 2C).

We investigate this region using a conventional pump-probe measurement with fixed amplitude pulses. Figure 3A shows the probe pulse current contribution as the pump-probe delay

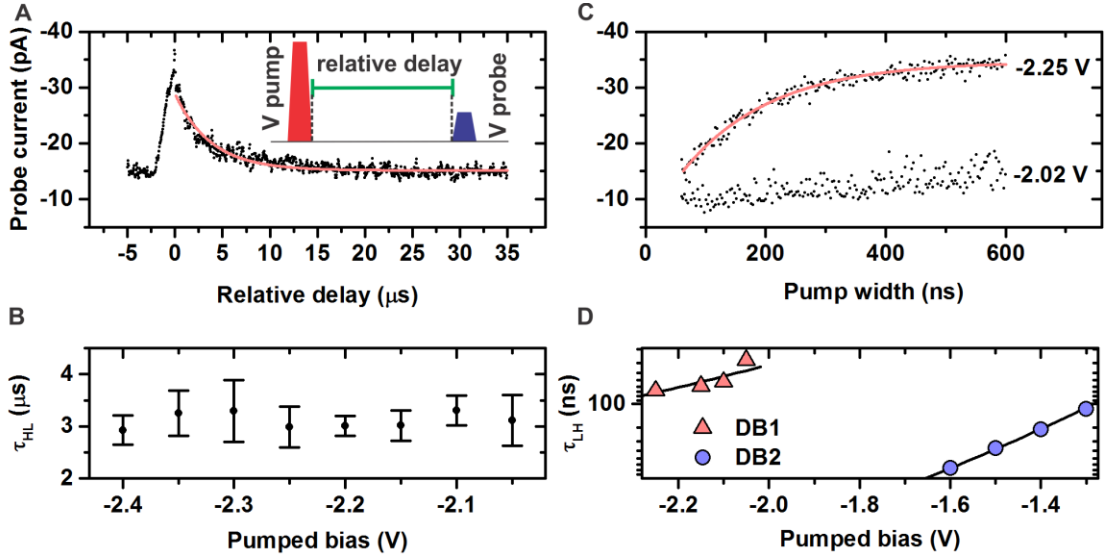


Fig. 3. Time resolved STM measurements of τ_{HL} and τ_{LH} . (A) τ_{HL} measurement from a 1 μs width probe pulse and a 1 μs width preceding pump pulse with repetition rate of 25 kHz at different relative delays. The probe (pump) amplitude is 0.21 V (0.40 V). With the DC offset set at -1.80 V, the probe and pump pulses are at -2.01 V and -2.20 V, respectively. The green bar in the inset indicates the relative delay, which is defined as the time between the trailing edge of the pump pulse and the leading edge of the probe pulse. (B) Measured τ_{HL} for different pump amplitudes shows that the time constant is independent of the pump bias. (C) τ_{LH} measurements at different pumped bias voltages (-2.02 V and -2.25 V shown as two examples) using a variable width pump pulse. The DC offset is -1.80 V, pulse amplitudes are the same as in A, the probe width is 1 μs and the relative delay is 10 ns. Red curves in (A) and (C) are the exponential fits. (D) τ_{LH} at different pumped bias voltages for the DB in Fig. 1 (denoted here as DB1) and for DB2 which is fully described in the supplementary material. Solid lines are the fits using Equation 1.

is swept. The DB is excited to a state with higher conductance by the pump, and subsequently relaxes back to the low conductance state. The relaxation can be fit with a single exponential decay function to extract the time constant of the high-to-low relaxation, τ_{HL} . Between pump voltages of -2.4V and -2.05V we find an approximately constant lifetime of $\tau_{HL}=3.1\pm 0.1 \mu\text{s}$ (Fig. 3B). We do, however, see an offset current; the low conductance state is not ~ 0 . Such a contribution is consistent with the pump pulse simultaneously exciting both the fast dynamics, and slow dynamics seen in telegraph noise.

To probe the excitation dynamics, we perform a pump-probe experiment varying the pump length and probing at a fixed delay (see Supplementary material for details). Figure 3C shows increasing probe pulse current contribution as the pump pulse widens. This measures the time constant of the excitation to the high conductance state during the pump, τ_{LH} . Unlike τ_{HL} , τ_{LH} shows an exponential dependence on the pump amplitude (Fig. 3D).

The results in Fig. 3C and D can be understood in terms of tunnel ionization of a neutral dopant in the field of the STM tip. At negative sample bias dopants in the surface region are below the Fermi level. However, due to non-equilibrium situation as a result of the depletion of surface dopants, beyond a critical voltage the emptying rate exceeds the supply of electrons from

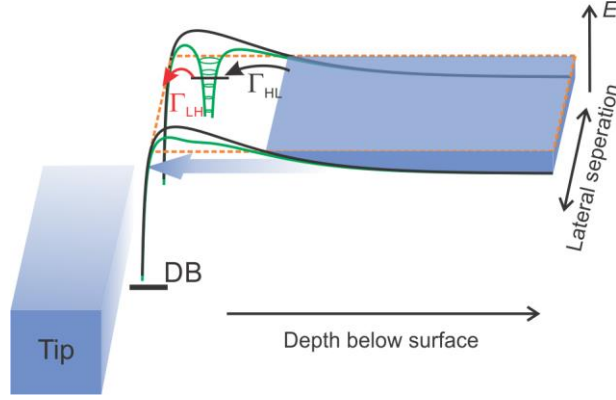


Fig 4. Diagram of the conduction band edge with and without an ionized dopant in the vicinity of a dangling bond. The conduction band edge in absence of an ionized dopant (black curve) rises in the near surface vicinity as a result of the depletion of dopants in that region, and falls precipitously as a result of TIBB. The green contour describes conduction band edge modified by the field of a nearby ionized dopant. The blue shaded area indicates the degenerately doped region. The black and red arrows show the neutralization rate from the bulk and ionization rate to the surface, respectively. The blue arrow represents the measured current, originating from the bulk conduction band as a result of lower barrier height (in green).

the bulk, rendering the ionization of the isolated near-surface dopants. As arsenic is a hydrogenic dopant in Si, the tunnel ionization time constant can be approximated as (21):

$$\tau_{LH} = \frac{\hbar e^3 F}{128\pi\epsilon E_{As}^3} \exp\left(\frac{32\pi\epsilon E_{As}^2}{3e^3 F}\right) \quad (1)$$

where E_{As} is the binding energy of the As dopant and ϵ is the dielectric constant of silicon. The ionization rate depends exponentially on the local electric field strength, F , at the dopant. The field strength experienced by a dopant in the depletion layer depends on its local environment and the electric field arising from tip induced band bending (TIBB) (21). Hence, the tip-induced electric field at any dopant increases proportionally to the applied bias and may be approximated as $F = \kappa|V_s| + F_0$, where κ is a proportionality factor relating the electric field to the applied bias, and F_0 is a constant field offset that includes the contact potential difference between tip and Si surface and interactions with nearby ionized dopants. This model accurately describes the observed switching rates shown in Fig. 3D: τ_{LH} depends exponentially on bias for both DBs shown but the rates are offset in bias as expected for different local dopant distributions.

The detection mechanism of the dopant dynamics can be explained by taking into account the effect of TIBB, the donor-depleted layer, and the effect of the electrostatic field of the ionized dopants on the CB edge. As a result of the dopant depletion region the degenerately doped bulk does not extend to the surface and the CB edge presents a potential barrier separating the carriers in the degenerately doped region from the surface and the DB (Fig. 4). This potential barrier accounts for the weak supply of electrons from the bulk to the DB for sample biases less negative than the critical voltage. As the critical voltage is crossed, we associate the sudden change in the supply rate of the DB with dopant ionization in the tip field, as similar systems

have been previously (3–6). The electrostatic effect of the ionized dopant significantly reduces the potential barrier which can lead to an increase in the conductivity from bulk to surface (Fig. 4). The magnitude of the influence of a nearby dopant may be estimated by computing transmission through a barrier modelled after the CB, and including the depletion layer. A few meV shift in the barrier height can increase transmission by multiple orders of magnitude (See supplementary material for details). The observed dynamics are therefore attributed to individual subsurface dopants, which gate the bulk-to-surface current. Donor ionization is exponentially dependent on the applied bias (Fig. 3D and Equation 1), but donor supply is determined by the local environment and is roughly independent of bias (Fig. 3B). Therefore, the onset of current occurs in a narrow transition region near the critical voltage where ionization overtakes donor supply. We also note that these same processes also describe the standard I(V) STS measurements through the DB. Variation in DB-dopant separation leads to variation in the opening voltage of this channel among individual DBs (19).

This model permits a robust description of the dynamics observed and demonstrates that the sharp tunneling current features stem from the gating influence and ionization thresholds of nearby dopants. More importantly, in conjunction with the ability of TR-STM to identify discrete voltage thresholds triggering separate time scales of dynamics, the model permits the disentanglement of the influence of multiple dopants. Here we analyze a case with two dopants, one slow, and one fast with as an example that captures a broad range of behavior. However, the range of variability in numbers and interactions of nearby dopants readily explains the wide range of critical voltages and sets of multiple current steps seen in DC measurements of DBs (19).

The Si surface DB is a convenient and powerful probe for dynamics of local dopants that may be used with TR-STM to understand complex environments. The combined technique and system has great potential in exploring the effects of sparse dopants in transistors, and in prototyping novel devices based on interacting or isolated dopants.

References and notes:

1. P. M. Koenraad, M. E. Flatté, Single dopants in semiconductors. *Nat. Mater.* **10**, 91–100 (2011).
2. A. Morello *et al.*, Single-shot readout of an electron spin in silicon. *Nature.* **467**, 687–691 (2010).
3. J. A. Mol, J. Salfi, J. A. Miwa, M. Y. Simmons, S. Rogge, Interplay between quantum confinement and dielectric mismatch for ultrashallow dopants. *Phys. Rev. B.* **87**, 1–7 (2013).
4. F. Marczinowski *et al.*, Local Electronic Structure near Mn Acceptors in InAs: Surface-Induced Symmetry Breaking and Coupling to Host States. *Phys. Rev. Lett.* **99**, 157202 (2007).
5. J. Salfi *et al.*, Spatially resolving valley quantum interference of a donor in silicon. *Nat. Mater.* **13**, 605–10 (2014).
6. B. Voisin, J. Salfi, J. Bocquel, R. Rahman, S. Rogge, Spatially resolved resonant tunneling on single atoms in silicon. *J. Phys. Condens. Matter.* **27**, 154203 (2015).

7. A. A Khajetoorians *et al.*, Detecting excitation and magnetization of individual dopants in a semiconductor. *Nature*. **467**, 1084–1087 (2010).
8. D. Kitchen, A. Richardella, J.-M. Tang, M. E. Flatté, A. Yazdani, Atom-by-atom substitution of Mn in GaAs and visualization of their hole-mediated interactions. *Nature*. **442**, 436–439 (2006).
9. K. Teichmann *et al.*, Bistable charge configuration of donor systems near the GaAs(110) surfaces. *Nano Lett.* **11**, 3538–42 (2011).
10. G. Nunes, M. R. Freeman, Picosecond resolution in scanning tunneling microscopy. *Science*. **262**, 1029–1032 (1993).
11. C. Grosse, M. Etzkorn, K. Kuhnke, S. Loth, K. Kern, Quantitative mapping of fast voltage pulses in tunnel junctions by plasmonic luminescence. *Appl. Phys. Lett.* **103**, 183108 (2013).
12. S. Loth, S. Baumann, C. P. Lutz, D. M. Eigler, A. J. Heinrich, Bistability in atomic-scale antiferromagnets. *Science*. **335**, 196–9 (2012).
13. S. Yan, D.-J. Choi, J. A. J. Burgess, S. Rolf-Pissarczyk, S. Loth, Control of quantum magnets by atomic exchange bias. *Nat. Nanotechnol.* **10**, 40–45 (2014).
14. C. Saunus, J. Raphael Bindel, M. Pratzner, M. Morgenstern, Versatile scanning tunneling microscopy with 120 ps time resolution. *Appl. Phys. Lett.* **102**, 051601 (2013).
15. I. Moul, M. Herve, Y. Pennec, Ultrafast spectroscopy with a scanning tunneling microscope. *Appl. Phys. Lett.* **98**, 233103 (2011).
16. S. Loth, M. Etzkorn, C. P. Lutz, D. M. Eigler, A. J. Heinrich, Measurement of fast electron spin relaxation times with atomic resolution. *Science*. **329**, 1628–30 (2010).
17. M. Berthe *et al.*, Electron transport via local polarons at interface atoms. *Phys. Rev. Lett.* **97**, 1–4 (2006).
18. J. L. Pitters, P. G. Piva, R. A. Wolkow, Dopant depletion in the near surface region of thermally prepared silicon (100) in UHV. *J. Vac. Sci. Technol. B.* **30**, 021806 (2012).
19. H. Labidi *et al.*, Scanning tunneling spectroscopy reveals a silicon dangling bond charge state transition. *New J. Phys.* **17**, 073023 (2015).
20. M. Taucer *et al.*, Single-Electron Dynamics of an Atomic Silicon Quantum Dot on the H-Si(001)-(2×1) Surface. *Phys. Rev. Lett.* **112**, 256801 (2014).
21. R. M. Feenstra, Electrostatic potential for a hyperbolic probe tip near a semiconductor. *J. Vac. Sci. Technol. B.* **21**, 2080–2088 (2003).
22. M. Rezeq, J. Pitters, R. Wolkow, Tungsten nanotip fabrication by spatially controlled field-assisted reaction with nitrogen. *J. Chem. Phys.* **124**, 204716 (2006).
23. J. J. Boland, Scanning tunnelling microscopy of the interaction of hydrogen with silicon surfaces. *Adv. Phys.* **42**, 129–171 (1993).
24. A. Hoffmann, M. T. Woodside, Signal-Pair Correlation Analysis of Single-Molecule Trajectories. *Angew. Chemie Int. Ed.* **50**, 12643–12646 (2011).
25. J. Wagner, J. A. Del Alamo, Band-gap narrowing in heavily doped silicon: A comparison

of optical and electrical data. *J. Appl. Phys.* **63**, 425–429 (1988).

Acknowledgments: We would like to thank Martin Cloutier and Mark Salomons for their technical expertise. We also thank NRC, NSERC, and AITF for financial support. J.A.J.B. acknowledges postdoctoral support from NSERC and the Alexander von Humboldt Foundation.

Supplementary Materials for

Time-Resolved Single Dopant Charge Dynamics in Silicon

M. Rashidi*, J. A. J. Burgess, M. Taucer, R. Achal, J. L. Pitters, S. Loth, and R. A. Wolkow

*correspondence to: rashidi@ualberta.ca

Materials and Methods

Methods

Measurements were performed using an Omicron LT-STM and Nanonis control system at a temperature of 4.5 K with a base pressure of 5×10^{-11} Torr. The STM is commercially equipped with radio frequency (RF) wiring with a bandwidth of ~ 500 MHz. The tungsten tips were chemically etched and cleaned and sharpened by electron beam heating followed by field ion microscopy (22). The samples were cleaved from a 3–4 m Ω .cm n-type arsenic doped Si(100) wafers (Virginia Semiconductor Inc.). They were degassed for several hours at 600°C and were cleaned by multiple flash annealing to approximately 1250°C then hydrogen-terminated near 330°C (23). The high temperature flash anneal depletes dopants in a surface region 60 nm wide as measured by SIMS (18). $I(V)$ spectra were measured in constant-height mode and tip quality was checked by performing reference spectroscopy on bare silicon and bare dimer defects. Voltage pulses and gentle, controlled contacting of tip to sample was used to improve the tip quality for STM imaging and spectroscopy in-situ.

Time-resolved Scanning Tunneling Microscope Setup

As shown schematically in Fig. S1, cycles of voltage pulse pairs were generated by an arbitrary function generator (AFG), Tektronix AFG3252C, summed (Mini-Circuits ZFRSC-42-S+), and fed into the tip. The DC bias voltage was applied to the sample and the tunneling current was collected through an Omicron preamplifier, connected to the sample. Two RF switches (Mini-Circuits ZX80-DR230-S+) connected to AFG output channels were used to either ground the tip during STM imaging and spectroscopy or connect the tip to the AFG during pump-probe measurements.

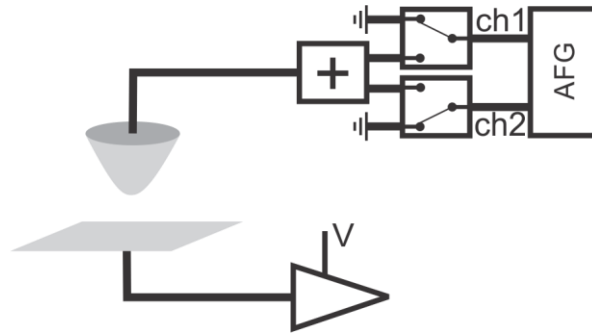


Fig. S 1 Time resolved scanning tunneling microscopy setup. An arbitrary function generator is the source of the pump and probe pulse trains which are applied to the STM tip. Two RF switches are used to turn on and off either pulse train.

The Auto-correlation signal measured on H:Si was used to monitor the quality of the pulses at the tunnel junction. Ringing is a common problem in this technique due to the imperfect impedance match between the tunnel junction and 50Ω impedance of the rest of the setup (11). To mitigate the ringing, 25 ns wide pulse edges were used throughout this work.

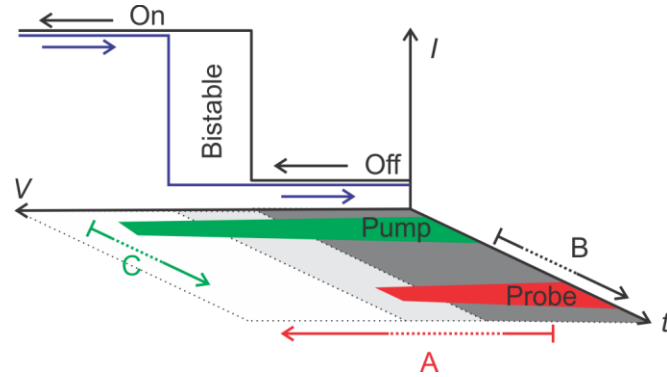


Fig. S 2 The phase space of parameters tuned in the presented time resolved measurements. As a background, (A) Time-resolved I(V) spectroscopy: tunneling current is measured from a series of varying-amplitude probe-pulses with and without a preceding pump pulse. (B) τ_{HL} measurement: a pump pulse is applied and a preceding probe pulse at different relative delay checks the status of the system at a bistable sample bias. (C) τ_{LH} measurement: A pump pulse with varying width is applied and a preceding probe pulse shortly after checks the status of the system at a bistable sample bias.

Time-Resolved Measurements

For time resolved measurements, tunneling current is induced by a series of short voltage pulses rather than by continuous DC bias. A significant number of parameters can vary for the measurement. Pulse amplitude, pulse width, repetition rate, delay between pump/probe pulse pairs and total measuring time can be adjusted depending on the nature of the measurement. Adjustments to parameters for TR-STM measurements used in this work are shown schematically in Fig. S2. Measurements fall into three categories, as detailed in the subsequent sections.

Time-Resolved I(V) Spectroscopy

The transient current spectrum taken as a function of bias voltage, $I(V, t)$, can be probed using a pump pulse to trigger dynamics, following with a probe pulse, and varying the amplitude of the probe. We exploited this as a technique using a fixed delay, with the probe pulse following as soon after the pump as our experimental apparatus permitted (10 ns between pulse edges), as a search tool to look for dynamical effects beyond our STM bandwidth as a function of bias. This corresponds to the configuration A in Fig. S2: the probe amplitude is swept while the delay, pulse widths, and pump amplitude are fixed. In the case of dynamic response, deviations between I(V) curves acquired with and without a pump pulse occur. This mode is then an efficient search tool. .

Time Constant Measurement of Transition from High to Low Conductance State

As shown schematically in Fig. S2B, to measure the time constant of the transition from high to low conductance (τ_{HL}), the DC offset is set at a sample bias voltage where the system is in the low conductance state (LC). A pump pulse brings the system to the high conductance (HC) state

and a subsequent probe pulse at different relative delays probes the status of the system at a sample bias at which bistability occurs. Within the relative delay time the applied bias is the DC offset, which has the effect of bringing the system to the LC state. At zero relative delay, the system is in the HC state. As the relative delay is increased, the system transitions to the LC state. The time constant of the exponential decay, is a measure of the characteristic time over which the system randomly transitions from the HC state to the LC state.

Time Constant Measurement of Transition from Low to High Conductance State

The schematic of time constant measurement for transition from low to high conductance state (τ_{LH}) is shown in Fig. S2C. A pump pulse with varying width is applied to bring the system to the HC state, and a subsequent probe pulse shortly after checks the state of the system at a sample bias at which bistability is observed. In order to calculate the current from the probe pulse only, for each pump width, the signal is measured with a small amplitude probe pulse and the result is subtracted from the measured signal with the probe pulse at the bistable bias range. A DC bias offset is applied at sample biases less negative than the bistable bias range to bring the system to the LC condition in the intervening time between pump-probe pairs. For short pump width, the system stays “off” and the probe current is almost zero. By increasing the pump width the average probe current increases exponentially and reaches its maximum value. The time constant of the exponential increase gives the time needed to pump the system, τ_{LH} . Since the current is almost zero at the DC offset, the measured tunneling current from the preamplifier comes almost exclusively from current during the time when the pulses are on. In order to obtain the actual current from the probe pulse, the measured current from the preamplifier is divided by the duty cycle of the pulse series and the current from the pump pulse is subtracted from that. The close match between this calculated current of the transient $I(V)$ and the current obtained by DC $I(V)$ at bias voltages outside the bistable region provides further evidence that the current comes predominantly from the pulses.

Signal Pair Analysis of Slow Transitions in the Bistable Energy Regime

The transition rates between the HC and LC states were calculated using a form of signal-pair analysis (24). The current-traces were placed in histograms and the HC and LC states were fit with Gaussian functions similar to Ref. (20). Regions of the histograms within each state were selected where the contributions from other states were minimized. Correlations were then calculated between these selected regions based on a linear transition pathway. The transition rates were determined directly from the fit of derived correlation functions (24) to these generated correlation data.

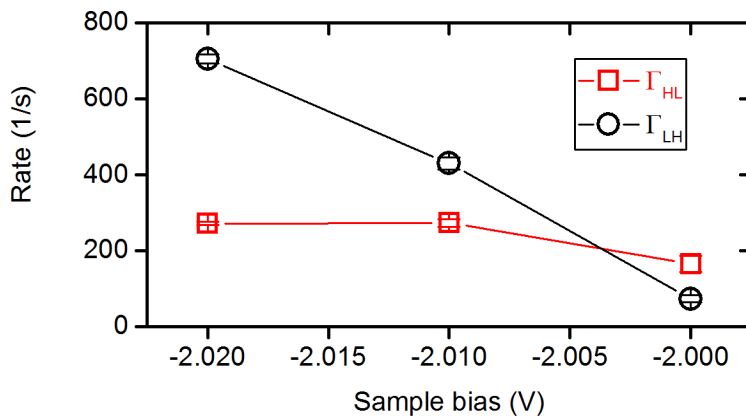


Fig. S 3 Rates from telegraph data in the bistable energy regime, calculated by signal pair analysis method.

Additional Example: TR-STM on a slow switching DB

The spectroscopic characteristics of DBs on samples prepared by heating to 1250°C, diverges because of the variation in their local environment (19). Therefore, we show another example here to illustrate that while the measured rates among different DBs are quantitatively different, different DBs qualitatively exhibit similar behavior. We present a DB (denoted as DB2 in Fig. 3D of the main manuscript) with the sharp current onset at ~ -1.15 V and with the transitions in the bistable energy regime in the range of seconds. This is very different from the DB studied in the main manuscript, which exhibits the current onset at ~ -2.00 V and transition rates in the bistable energy regime of a few hundred hertz. The slow transitions at this DB lead to hysteresis in forward and backward I(V) sweeps (Fig. S4) when the total sweep time is less than a few seconds. Only for relatively slow measurements (sweep time of ~ 6.5 s) does the hysteresis loop vanish.

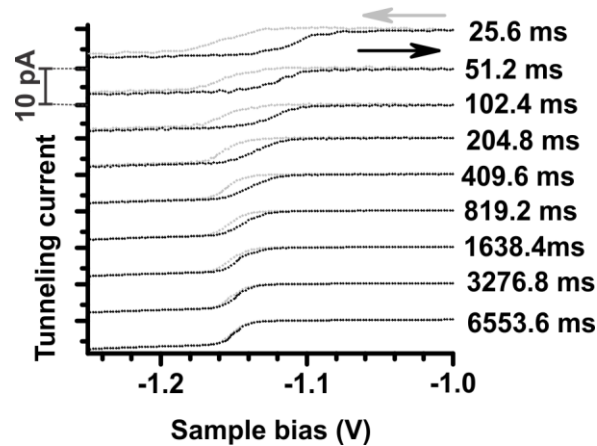


Fig. S 4 Forward (-1.2 V to -1.0 V) and reverse bias spectroscopy sweeps in the case of a DB with slow time dynamics reveals conductance hysteresis. The I(V) curves are the averages of 100 sweeps at different total sweep times indicated on the side of each curve. The hysteresis loop closes for sweep times around 6.5 s, indicating dynamics in the range of hertz at the transition bias.

Figure S5 displays TR-STTS on this DB. The TR-STTS shows a wider hysteresis loop than any of the conventional STS sweeps, in agreement with the trend of widening of the hysteresis loop for faster $I(V)$ sweeps observed in Fig. S4. The time-resolved spectra measured with and without the pump pulse are analogous to forward and reverse sweeps of the conventional spectra shown in Fig. S4, respectively.

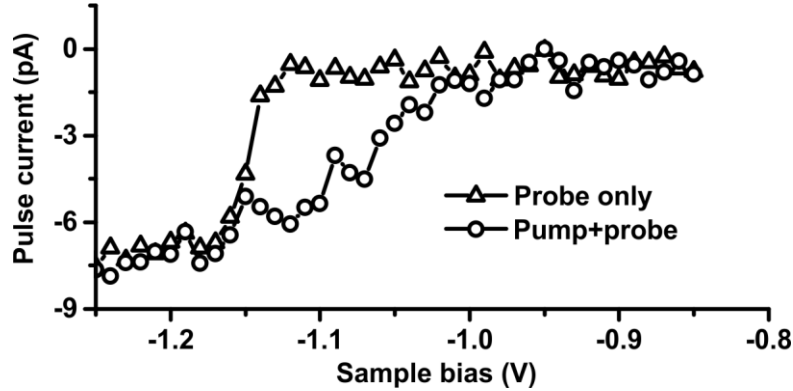


Fig. S 5 TR-STTS on the DB in Fig. S4. Current from a $1 \mu\text{s}$ width probe pulse with and without a $10 \mu\text{s}$ width preceding pump pulse. The delay from the trailing edge of the pump pulse to the leading edge of the probe pulse is 10 ns and the DC bias voltage is set at -0.80 V . The amplitude of the pump pulse is 0.60 V and that of the probe pulse is swept from 50 to 450 mV . Since the polarity of both pulses is negative, the pumped bias is -1.40 V and the probe sweeps the bias range of -0.85 to -1.25 V .

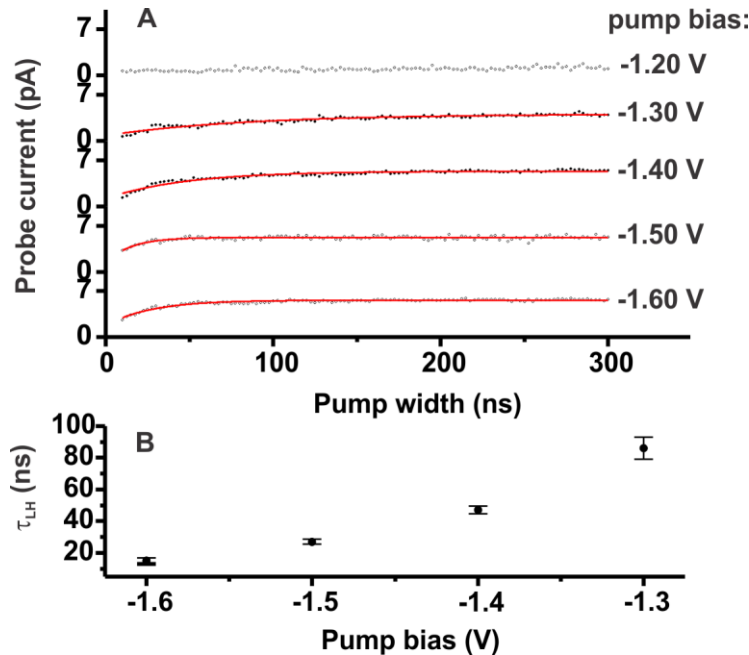


Fig. S 6. (A) TR-STM measurement of τ_{LH} at different pump bias on the DB in Fig. S4. The DC offset is -0.80 V . The probe width and relative delay is $1 \mu\text{s}$ and 10 ns , respectively. Red curves are exponential fits. (B) τ_{LH} vs. pumped bias.

Calculation of Conduction Band Edge and Transport Mechanism from the Bulk to the Surface

For samples prepared by heating to 1250°C, secondary ion mass spectrometry (SIMS) shows substantial near surface depletion of dopants (18, 19). As a result, the degenerately doped region does not extend to the surface. The band gap narrowing in heavily doped silicon as function of dopant concentration can be empirically expressed as (25)

$$\Delta E_G = 18.7 \times 10^{-3} \ln(N_D / 7 \times 10^{17} \text{ cm}^{-3}) [\text{eV}],$$

where N_D is the dopant concentration.

The black curve in Fig. S7 shows the conduction band (CB) edge calculated near the surface vicinity by considering the band gap narrowing, tip induced band bending (TIBB) (21) and the dopant concentration profile from SIMS measurements (18). The CB edge first rises as a result of the depletion of dopants in that region, and falls rapidly as a result of TIBB at the surface, acting as an energy barrier for the electrons to conduct from the bulk (degenerately doped region) to the surface. The electrostatic potential due to an ionized dopant lowers this energy barrier (green curve in Fig. S7), increasing the electron conductivity from the bulk to the surface.

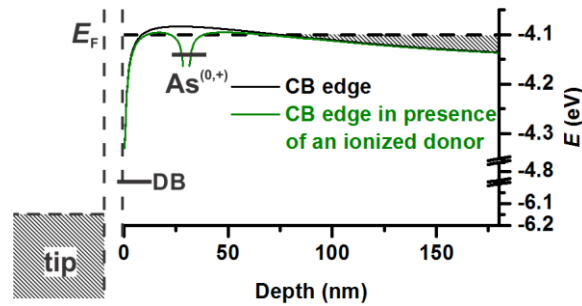


Fig. S7 Conduction band edge in presence (green curve) and absence (black curve) of an ionized dopant computed for the sample bias voltage of -2.0 V.

The magnitude of the effect of the field of an ionized dopant on the tunnel current observed at a DB may be estimated by an approximate calculation. The electrostatic influence of a nearby dopant can lower the maximum height of the barrier to less than 5 meV. Using the CB shape computed with dopant depletion and TIBB, the transmission coefficient describing transport from the bulk to the surface can be estimated using the WKB approximation. Adding dopants separated from the DB by a few nanometer up to a few 10's of nanometer, shows transmission through the barrier may increase by orders of magnitude upon ionization of the dopant (Fig. S8). Additionally the population of thermally excited electrons in the CB rises significantly for barriers of less than 5 meV at our experimental temperature (4.4K). Either, or both, of these mechanisms can explain the electron transport from the bulk to the surface through the energy barrier and the observed sudden current turn on in I(V) spectroscopy.

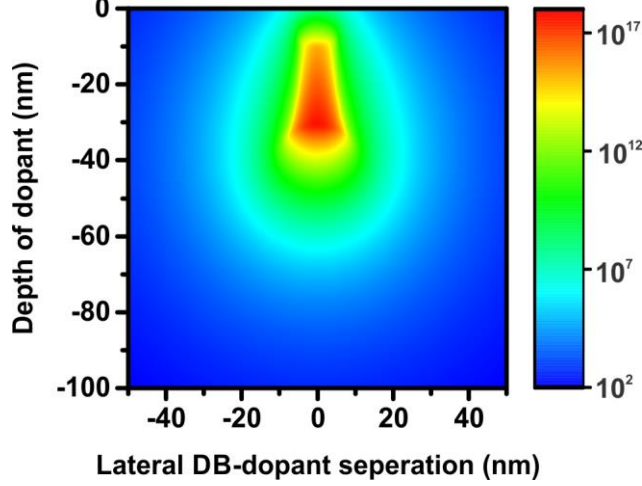


Fig. S8 Color-map of the tunneling transmission coefficient through the energy barrier between the degenerately doped bulk CB and the surface resulting from dopant ionization at different depth, and lateral position from a DB. The weights were calculated using WKB approximation. The sample bias voltage is set to -2.0 V. The tip and DB are placed at $(0,1$ nm) and $(0,0)$, respectively.

Theoretical Treatment of Tunnel Ionization of Neutral As Donors

Donors are ionized in the field of the tip. The bound electron tunnels through a roughly triangular barrier formed by the confining potential of the host donor and the tilted potential of the field, as shown in Fig. S9A. Ionization rate is a function of field strength, which can be derived analytically for the Hydrogen atom,

$$\Gamma_{ion}(F) = \frac{4m^3 e^9}{\hbar^7 F} \exp\left[\frac{-2m^2 e^5}{3\hbar^4 F}\right].$$

To treat the case of an arsenic donor in silicon, we adapt this relation and express it in terms of the binding energy, as

$$\Gamma_{ion}(F) = \frac{128\pi\epsilon E_{bind}}{\hbar e^3 F} \exp\left[\frac{-32\pi\epsilon E_{bind}}{3e^3 F}\right],$$

which is the inverse of the time constant, τ_{LH} , in equation (1) of the manuscript. The binding energy and dielectric constant in this equation are modified from the case of the hydrogen atom in vacuum to reflect the binding energy of the As donor and the dielectric constant of silicon. This form of the ionization rate as a function of field strength does not explicitly include the effective mass of the electron, instead using the known binding energy of 54 meV. This is done since the effective mass treatment of an electron donor in silicon underestimates the binding energy by a factor of nearly two. Since the binding energy plays a very important role in determining the rate of tunnel ionization, we choose to insist on this quantity in our treatment of donors.

Fig. S9(B) shows ionization as a function of field strength. The rate increases non-linearly, and within the fields that can be experienced by near-surface donors, we see that there is a

dramatic change in the ionization rate from effectively zero, to much faster than the timescales that are accessible in STM experiments, shown as shaded regions in the inset of Fig. S9(B). The sharp transition studied in this paper is due to this rapid transition in rates as the field experienced by individual donors increases.

As the sample bias becomes increasingly negative in an STM experiment, the tip has an increasing field effect on nearby donors (although the effect of contact potential must also be taken into account). The field eventually becomes large enough to ionize a donor, making it positively charged. As the field increases further, deeper donors may ionize. These deeper donors, however, experience an additional field due to the positive charge of already-ionized donors nearer to the surface. The field experienced by a sub-surface dopant can therefore be approximated as a linear function of sample bias, subject to an offset due to previously ionized dopants, as well as an offset due to the contact potential difference (CPD) between the tip and the sample.

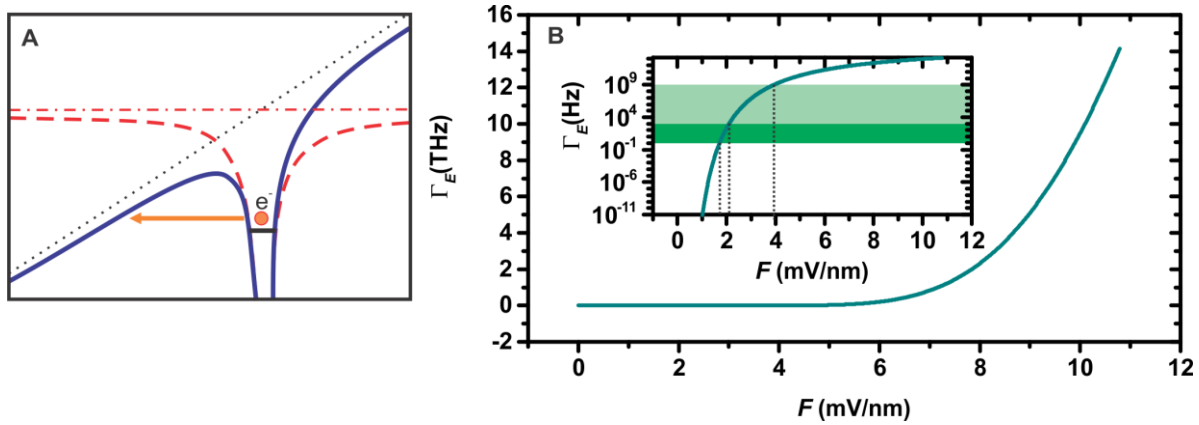


Fig. S 9 (A) The arsenic donor can be stripped of its bound electron through tunnel ionization in the presence of a field. (B) Ionization rate as a function of field strength. Inset shows a semi-logarithmic plot with the dark shaded region indicating the typical timescales for standard STM measurements. The lighter shaded region indicates the timescales that are accessible in TR-STM.